Effect of cavity architecture on the surface enhanced emission from site selective nanostructured cavity arrays

Frances Lordan, James H Rice
School of Physics, University College Dublin, Belfield, Dublin 4, Ireland

Bincy Jose, Robert J Forster, Tia E Keyes
School of Chemical Sciences, Dublin City University, Dublin 9, Ireland

Presented here are studies of the impact of incident angle on surface enhanced emission from a dye that is located site selectively on a plasmon active nanocavity array support. Studies were performed for a surface active luminescent dye selectively assembled on the top surface or on the walls of the voids of nanocavity array substrates. Results show that emission intensities depend on where the dye is located with respect to the void or surface of the nanocavity array and on the dimensions of the cavity. This was interpreted to arise from the presence of void localised plasmons and surface localised and delocalised plasmon modes.

Corresponding author
James rice@ucd.ie

1. Introduction

Emission spectroscopy and microscopy such as those of fluorescence based methods are widely applied in sensing/ analysis and in materials characterization. Increasing the emission signal intensity is attractive for many applications as it can lead to increased analytical sensitivity. One approach used to enhance emission signal strength is to use plasmon active substrates. Metal enhanced fluorescence or, more generally, luminescence potentially enhances the emission from the target system (surface enhanced luminescence (SEL)), via a mechanism similar to that for surface enhanced Raman (SERS) [1,2]. Enhancing luminescence signal is a more complicated proposition however, as metal surfaces can quench as well as enhance luminescence. A well-studied approach to generate SEL and SERS is to use spherical metallic nanoparticles or roughened metallic surfaces to generate a plasmon active substrate [3,4,5]. These materials are predicted to enable signal enhancement up to 10^5 for SERS [6]. However the presence of localized "hot spots" with enhancements in excess of 10^{10} has been reported for SERS [7]. There is a lack of complete control over the size and shape of metallic particles/features formed, leading to irreproducibility of SEL or SERS signal enhancement. Methods using lithography such as electron beam based approaches have been used to create reproducible plasmon active surface features [8]. However, the high costs associated with this approach have prevented wide scale use.

Reproducible plasmon active substrates based on nanosphere lithographic fabrication methods have been quite widely reported. The resulting structures have nanovoid architecture such as those reported here. The nanostructured surfaces studied here have spherical cap architectures and are arranged uniformly in a hexagonally close-packed Au array. Au is commonly used for plasmonic platforms as it produces chemically and structurally stable high quality arrays with visible and NIR plasmonic absorbance. Furthermore, Au nanocavity arrays tend to be more reproducible and homogeneous than arrays made from other materials e.g. Ag [9]. These structures support both localised and delocalised plasmons. Localised surface plasmon polaritons (LSPPs) exist inside the nanocavities (Mie plasmons) and localised and delocalised or propagating surface plasmon polaritons (PSPPs) exist on the flat surface of the sample (Bragg plasmons) [10]. Studies on localised and delocalised plasmons have been carried out by Kelf et al. in which the separate contributions of the different plasmon types were investigated by varying the normalised sample film thickness. Other interesting studies on nanocavity arrays have been carried out by Chan et al in which the effect of cavity diameter on the SERS intensity from a Ag array was investigated [11]. Another application of these substrates is as platforms for SEL [12,13]. This area has been less widely studied than SERS, particularly on these types of ordered architecture. However, a few studies have been carried out on both the angle dependence of SERS [14] and SEL [13]. from plasmon active nanocavity arrays. These studies show that both SERS and SEL are dependent on the angle of laser incidence and/or detection angle, a consequence of the coupling of the excitation line to different plasmon modes with angle. This angle dependence is used in this work to enable comparison between SEL and surface enhanced resonance Raman scattering (SERRS) of $[Ru(bpy)_2(Qbpy)]^{2+}$ caused by localised plasmons in the voids and SEL and SERRS caused by plasmons located on the substrate surface.

Several studies have been reported demonstrating SERS using nanovoid cavity substrates [14-18]. Baumberg et al [14] showed strong correlations between plasmon resonances and Raman

enhancements by studying different cavity dimensions as a function of incident angle. Sugawara et al [12] studied nanovoid samples coated with organic semiconducting molecular *J*-aggregate films. This study showed room temperature excitonic luminescence is enhanced by plasmonic coupling using nanovoid substrates. Studies of the emission of dye absorbed to the surface of nanovoids have been carried out [2]. Nanovoid substrates were reported to support Mie or Bragg plasmons depending on the dimensions of the nanovoids themselves [19]. Bragg plasmons were shown to be present for thin films while localised Mie plasmons are seen at larger thicknesses. The presence of such modes has been observed in the near-field using scanning tunneling microscopy (STM) [20].

In this present study the arrays were selectively modified by adsorbing a luminescent monolayer on different regions of the sample according to a nanosphere masking method reported recently [21]. In the externally modified array the probe is selectively assembled at the flat top surface of the array, whereas the internally modified array had dye placed only on the internal walls of the cavities. A blocking, non-luminescent alkane thiol is assembled at the top surface of this array. This enabled comparison of the luminescence spectra of the dye localised in the cavity and dye localised on the top surface of the array and comparison of the angle dependence of both spectra. Such a study has the potential to enable clearer understanding of the role that the void and the surface bound plasmon modes have on SEL.

Here studies of SEL and SERRS have been performed for molecule located on both the surface or in cavities of two different designs. One cavity having dimensions $\bar{t} = 0.95$ which is expected to result in the formation of LSPP modes localised both in the cavity (Mie plasmons) and also at the rim of the cavity at the surface (rim plasmon modes) and PSPPs modes on the surface of the nanocavity array [10]. A second cavity is studied with dimensions $\bar{t} = 0.12$ which is expected to result in the formation of PSPP modes both in the cavity (Bragg plasmons) and on the surface of the nanocavity array [10]. The probe molecules are only present on the internal cavity walls or on the surface of the array.

2. Experimental

Gold nanocavity arrays on silicon wafer were prepared using a nanosphere lithographic technique based on electrodeposition through the voids of self-assembled 430 nm or 820nm diameter polystyrene spheres on 50 nm thick gold films on silicon as described. Selective modification of the external edges and interior walls of the cavity arrays with $[Ru(bpy)_2(Qbpy)]^{2+}$ was achieved through a two-step adsorption process [21]. As outlined by Jose et al in instances where $[Ru(bpy)_2(Qbpy)]^{2+}$ is adsorbed selectively at the inner cavity walls, the top surface was first blocked with 1-nonanethiol before removal of the template [21]. These samples were then probed with Raman and luminescence spectroscopy to probe their site elective deposition [21]. The samples were first studied using scanning electron microscopy (SEM) and atomic force microscopy (AFM). The sample was mounted onto a customized goniometer at a tilted (azimuth) angle of 13.5 degrees. The sample was excited at 532 nm with the laser focused using a 10 cm focal length lens. The Raman and luminescence signals were collected at a backscattered angle and directed onto an electron multiplying charge coupled device (EMCCD) via a monochromator. The pump angle was varied in steps of 1^o and a

spectrum was taken at each step with the detection angle fixed. The lasers power was 20 mW over a post size of c.a. 1 micron. This was carried out for two cavity architectures. A 820nm diameter external modified and internal modified cavity array which possessed an aspect ratio (of depth of coverage to diameter) of $\bar{t}$ =0.12 [2,13]. A cavity formed from the 430nm diameter spheres possessed an aspect ratio (of depth of coverage to diameter) of $\bar{t}$ =0.95[2,13].

3. Results and discussion

Fig 1a shows schematically the likely location of different plasmon modes that occur on the nanovoid array substrates. The black lines shown on Fig 1a indicate the possible paths of SPs on the array (marked 1 and 2 in Fig 1a) along with void localised plasmons (marked 3 in Fig 1a). Line 1 shows the path taken by a localised SP; it is confined to the distance between the cavities. Live et al reported that PSPP may be confined in space by the boundaries in nanocavity arrays [22]. Alternatively localized surface plasmon modes may arise from hybrid rim-surface plasmon mode [23]. This localisation of the SP enables its contribution to the SERS spectrum. Line 2 shows a possible path taken by a PSPP. This line traverses flat gold and avoids the edges of the nanocavities, thereby avoiding confinement [22]. These delocalised SPs are expected to contribute little to SERRS as they cannot be excited at an air metal interface by incident light [16].

Fig 1d outlines the emission spectrum for $[Ru(bpy)_2(Qbpy)]^{2+}$ which emits from a triplet metal to ligand charge transfer state at 650 nm. Inspection of the absorption spectrum at 532 nm confirms an overlap with the excitation laser. This indicates that SERRS is produced at this wavelength. The emission spectrum shows a peak at c.a. 1.8 eV which, thanks to the larges Stokes shift of this dye, is to the red of the Raman window located at c.a. 2.15 eV. This permits simultaneous collection of both emission and resonance Raman data. SERRS spectra recorded using a 532 nm excitation wavelength are shown in Fig 1b. The Raman spectra show several peaks which are characteristic of pyridine modes observed previously from SERS spectra of $[Ru(bpy)_2(Qbpy)]^{2+}$ [2]. In addition the emission from $[Ru(bpy)_2(Qbpy)]^{2+}$ (shown in Fig 1c) was recorded simultaneously with the SERRS spectra. This emission is assigned to SEL i.e. plasmon assisted emission[2].

Fig 2 shows SEL and SERRS recorded from $[Ru(bpy)_2(Qbpy)]^{2+}$ assembled selectively at the voids walls of the 820 nm nanocavity array . The SEL band (centred at 1.76 eV) is much stronger than the SERRS features. The strongest SERRS band is at 2.14 eV. Fig 1b shows more closely the SERRS features recorded for $[Ru(bpy)_2(Qbpy)]^{2+}$ prepared in the voids of the array only. The most intense SERRS band is marked α in Figs 1b and 1c. The most intense part of the SEL spectrum is marked β in fig 1c. As cavity plasmon mode excitation is expected to be incident angle dependent, but plasmons at a roughened planar surface are not, [14] studies of the SEL intensity against angle of incidence as a function of location of the dye were undertaken. Monitoring the change in the intensity of the emission with incident angle confirms that the intensity of the emission at β depends upon angle. The intensity profile shows regions of relatively high emission signal and regions of relatively low emission signal which vary with θ. Fig 2b shows a plot of intensity for energies corresponding to α and also β at varying angles of incidence for the interior modified array. These plots are shown in more detail in Figs 2c and 2d

for clarity. Figs 2 c and 2d shows for both the emission and the Raman an increase in intensity from $\theta = 0^o$ to c.a. $\theta = 25^o$, followed by a decline in intensity from θ = c.a. 25^o to $\theta = 40^o$ where the experimental observation ends.

Fig 3 shows SEL and SERRS recorded from $[Ru(bpy)_2(Qbpy)]^{2+}$ prepared on the surface of the nanovoid only for the 820 nm nanocavity array. Monitoring the change in the intensity of the emission shows that the intensity of the emission at β depends upon angle. Fig 3b shows a plot of intensity for energies corresponding to α and also β at varying angles of incidence. These plots are shown in more detail in Figs 3c and 3d. These figures show that both the emission and the Raman decline in intensity from $\theta = 0^o$ to $\theta = 40^o$.

The intensities of the plasmons vary as a function of both θ and the frequency of incident EM radiation.[10] Both experimental and theoretical studies have indicated that the absorption energy of such cavity related plasmons change as a function of θ for angle of incidence [10,14,23]. The array has cavities with dimensions $\bar{t} = 0.12$ that are expected to result in the formation of cavity localised plasmons with localised standing wave of propagating SPPs or Mie-rim based hybrid dipole modes as well as SPP modes on the surface of the nanocavity array[10]. For the internally modified array the Raman active dye is only present on the internal cavity walls. This enables the study of the angle dependence of the SERRS spectrum where the enhancement is due to cavity localised plasmons and rim based hybrid localized plasmons. Different angle dependence is observed when the probe dye is placed on the top surface. This angle dependence arises from PSPP modes on the surface interacting with the dye or from rim based plasmon modes which may also be active on the surface. It is noted from inspection of Fig 1, the AFM topography image suggests that the surface of the substrate may be rough leading to LSPP on the surface which can couple with the probe dye leading to SERRS.

Fig 4a,b shows SEL and SERRS recorded from $[Ru(bpy)_2(Qbpy)]^{2+}$ prepared in the 430 nm voids of the nanocavity array only. The SEL band centred at 1.76 eV is much stronger then the SERRS features. The strongest SERRS band is at 2.14 eV. Studies of the SEL intensity against angle of incidence were undertaken. Monitoring the change in the intensity of the emission shows that the intensity of the emission at β depends upon angle. The intensity profile shows regions of relatively high emission signal and regions of relatively low emission signal which vary with θ. Fig 4b shows a plot of intensity for energies corresponding to α and also β at varying angles of incidence for the interior modified array for SERRS and SEL. Fig 4b shows the SEL increasing in intensity from $\theta = 0^o$ to c.a. $\theta = 40^o$. This rise is accompanied by undulating changes superimposed onto this rising profile. Fig 4b also shows the SERRS profile which increases in intensity from $\theta = 0^o$ to c.a. θ = c.a.25^o followed by a decline in intensity from θ = c.a. 25^o to $\theta = 40^o$ where the experimental observation ends.

SEL and SERRS recorded from $[Ru(bpy)_2(Qbpy)]^{2+}$ prepared on the surface of the 430 nm nanovoid substrates only are shown in Fig 4c,d. Fig 4c shows the SEL and SERRS spectrum. Fig 4d shows a plot of SEL intensity at α and β against angle of incidence. Monitoring the change in the intensity of the emission shows that the intensity of the emission at β depends upon angle. The intensity profile shows regions of relatively high emission signal and regions of relatively low emission signal which vary with θ. Fig 4d shows that both the emission and the Raman

follow a similar trend. The SEL intensity rises in intensity from $\theta = 0^o$ to $\theta = 40^o$. Fig 3b shows also the SERRS intensity as a function of angle. The SERRS intensity rises from $\theta = 0^o$ to $\theta =$ c.a. 30^o followed by a steadying in intensity from $\theta =$ c.a. 30^o to $\theta = 40^o$.

Comparing SEL intensity from $[Ru(bpy)_2(Qbpy)]^{2+}$ prepared in the voids of the 430 nm nanocavity array only to those prepared on the surface of the substrate shows a very similar changes in intensity as a function of angle. Studies of periodic cavity arrays proposed that there are different possible directions of PSPPs, whereby the propagation can be in one case confined between two neighbouring nanocavities, while in another case the surface plasmon is free to propagate in one direction for lengths potential larger than tens of microns, similar to propagating surface plasmon resonance on a continuous metallic film [22]. The presence of surface plasmons occurring in the short distance between adjacent nanocavities (annulus to localized surface plasmons) and a long axis between rows of nanocavities (comparable to propagating surface plasmons) was investigated using total internal reflection (TIF) measurements [22]. TIF produced evidence for the presence of both a short-range surface plasmon resonance and propagating surface plasmon resonances. As the size of the nanocavity is reduced the packing density of the spheres increases. This leads to the creation of reduced potential for free propagation distances on the surface of the substrate and an increase of confined areas or 'islands' between two neighbouring nanocavities. As the cavity sized is reduced the size of these islands decreases leading to increased localisation of surface located plasmons. The possibility that confinement of PSPPs by the presence of many small cavities on the surface resulting in LSPPs may occur with the 430 nm nanocavity sample may be present.

Comparing SEL intensity from $[Ru(bpy)_2(Qbpy)]^{2+}$ prepared only in the voids (Fig 4a,b) of the nanocavity array to those prepared only on the surface (Fig 4c,d) of the substrate shows no clear difference, with the signal intensity rising from $\theta = 0^o$ to $\theta = 40^o$. Comparing SERRS intensities shows a small difference with the SERRS intensity vs angle peaking with the cavity LSPPs at c.a. $\theta = 25^o$. This compares to a gradual rise to $\theta = 40^o$ in SERRS signal intensity for the surface bound molecule. These effects may arise from the surface LSPPs possessing similar properties to the cavity LSPPs with respect to enhancement of the signal at 1.76 eV. While at 1.82 eV (where the SERRS signal is monitored) the energy of the LSPPs may be different when they are localised in the cavity or on the surface. Inspection of the AFM topography image of the nanocavity (Fig 1d) shows that the surface of the nanocavity is not smooth. The nanovoid has been nearly filled in resulting in regions between the nanovoids which are sloped. Inspection of the AFM image shows that there are regular line patterns (marked 1) running between the nanovoids (marked 2). These create triangular shaped regions of c.a. 400 nm in length. This potentially aids in the creation of LSPPs on the surface. Studies of $[Ru(bpy)_2(Qbpy)]^{2+}$ prepared in 820 nm (larger and shallower) Bragg active cavities differences are seen when the molecule was prepared in the cavity or on the surface with respect to SEL and SERRS signal intensity as a function of angle [13,19]. This can be interpreted to arise from the presence of PSPPs that were freely propagating and not localised on a surface were the nanocavities were large enabling a long axis between rows of nanocavities.

5. Concluding remarks

Presented here are studies of angle dependent SERRS and SEL from a dye that is located site selectively on a plasmon active nanocavity array support. Results show that angle dependence of the emission intensities depend on where the dye is located with respect to the void or surface of the nanocavity array. In addition the architecture of the nanocavity array is shown to be important. Studies of different cavity dimensions showed indicated that the PSPP can be confined in certain cavity architectures creating LSPP modes.

5. Acknowledgements

This work was funded by Science Foundation Ireland and the Higher Educational Authority (HEA) Ireland.

6. References

[1] Tion, Z. Q.; Ren, B.; Wu, D. Y. Surface-Enhanced Raman Scattering: From Noble to Transition Metals and from Rough Surfaces to Ordered Nanostructures. J. Phys. Chem. B, **2002**, *106*, 9463-9465.

[2] Jose, B.; Steffen, R.; Neugebauer, U.; Sheridan, E.; Marthi, R.; Forster, R. J.; Keyes, T. E. Emission Enhancement within Gold Spherical Nanocavity Arrays. Phys. Chem. Chem. Phys, **2009**, *11*, 10923-10927.

[3]. Nie, S.; Emory, S. Probing Single Molecules and Single Nanoparticles by Surface-Enhanced Raman Scattering. Science, **1997**, *275*, 1102-1106.

[4] Kneipp, K.; Wang, K; Kneipp, H.; Perelman, L.; Itzkan, I. Single Molecule Detection Using Surface-Enhanced Raman Scattering (SERS). Phys. Rev. Lett., **1997**, 78, 1667-1670.

[5]. Muniz-Miranda, M.; Gellini, C.; Pagliai, M.; Innocenti, M.; Salvi, P. R.; Schettino, V.; SERS and Computational Studies on MicroRNA Chains Adsorbed on Silver Surfaces. J. Phys. Chem. C, **2010,** *114*, 13730-13731.

[6]. Kerker, M.; Siiman, O.; Bumm, L. A.; Wang, D. S. Surface enhanced Raman scattering (SERS) of citrate ion adsorbed on colloidal silver. App. Optics., **1980**, *19*, 3253-3255.

[7]. Xu, H.; Aizpurua, J.; Kall, M.; Apell, P. Electromagnetic contributions to single-molecule sensitivity in surface-enhanced Raman scattering. Phys. Rev. E, **2000**, *62*, 4318-4324.

[8]. Guicheteau, J.; Christesen, S.; Emge, D.; Wilcox, P.; Fountain, A. W. Semi-Automated Detection of Trace Explosives in Fingerprints on Strongly Interfering Surfaces with Raman Chemical Imaging. App. Spec., 2011, ***65***, 611-619.

[9]. Cortes, E.; Tognalli, N. G.; Fainstein, A.; Vela, A. M. E.; Salvarezza, R. C. Ag-modified Au nanocavity SERS substrates. Phys. Chem. Chem. Phys. **2009**, *11*, 7469-7475.

[10] Kelf, T. A.; Sugawara, Y.; Cole, R. M.; Baumberg, J.J.; Abdelsalam, M.E.; Cintra, S.; Mahajan, S.; Russell, A. E.; Bartlett, P. N. Localized and delocalized plasmons in metallic nanovoids. Phys. Rev. B. **2006**, *74*, 245415.

[11]. Chan, C. Y.; Xu, J. B.; Waye, M. Y.; Ong, H. C. Angle resolved surface enhanced Raman scattering (SERS) on two-dimensional metallic arrays with different hole sizes. Appl. Phys. Lett. **2010**, *96*, 33104-33107.

[12] Sugawara, Y.; Kelf, T. A.; Baumberg, J. J.; Abdelsalam, M. E.; Bartlett, P. N. Strong Coupling between Localized Plasmons and Organic Excitons in Metal Nanovoids. Phys. Rev. Lett. **2006**, *97***,** 266808.

[13]. Lordan, F.; Rice, J.H.; Jose, B.; Forster, R. J.; Keyes, T. E. Surface enhanced resonance Raman and luminescence on plasmon active nanostructured cavities. Appl. Phys. Lett. **2010**, *97*, 153110-153113.

[14]. Baumberg, J.J.; Kelf, T. A.; Sugawara, Y.; Cintra, S.; Abdelsalam, M.E.; Bartlett, P. N.; Russell, A. E. Angle-Resolved Surface-Enhanced Raman Scattering on Metallic Nanostructured Plasmonic Crystals. Nano Lett. **2005**, *5*, 2262-2267.

[15]. Abdelsalam, M. E.; Mahajan, S.; Bartlett, P. N.; Baumberg, J. J.; Russell, A. E. SERS at Structured Palladium and Platinum Surfaces. J. Am. Chem. Soc., **2007**, *129*, 7399-7406.

[16]. Mahajan, S.; Cole, R. M.; Soares, B. F.; Pelfrey, S. H.; Russell, A. E.; Baumberg, J. J.; Bartlett, P. N. Relating SERS Intensity to Specific Plasmon Modes on Sphere Segment Void Surfaces. J. Phys. Chem. C. **2009**, *113*, 9284-9290.

[17]. Mahajan, S.; Baumberg, J .J.; Russell, A. E.; Bartlett, P. N.; Reproducible SERRS from structured gold surfaces. Phys. Chem. Chem. Phys. **2007**, *9*, 6016-6020.

[18]. Lacharmoise, P. D. ; Tognalli, N. G. ; Goñi, A. R. ; Alonso, M. I.; Fainstein, A.; Cole, R. M. ; Baumberg, J.J.; Garcia de Abajo, J.; Bartlett, P. N. Imaging optical near fields at metallic nanoscale voids. Phys. Rev. B. **2008**, *78*, 125410.

[19]. Cole, R. M.; Mahajan, S.; Bartlett, P. N.; Baumberg, J. J. Engineering SERS via absorption control in novel hybrid Ni/Au nanovoids. Optics Express, **2009**, *17*, 13298-13308.

[20]. Mahajan, S.; Abdelsalam, M.; Suguwara, Y.; Cintra, S.; Russell, A. E.; Baumberg, J. J.; Bartlett, P. N. Tuning plasmons on nano-structured substrates for NIR-SERS. Phys. Chem. Chem. Phys. **2007**, *9*, 104-109.

[21]. Jose, B; Mallon, C. T.; Forster, R. J.; Keyes, T. E. Regio-Selective Decoration of Nanocavity Metal Arrays: Contributions From Localized and Delocalized Plasmons to Surface Enhanced Raman Spectroscopy. Phys. Chem. Chem. Phys. **2011**, *13*, 14705-14714.

[22]. Live, L. S.; Murray-Methot, M. P.; Masson, J. F. Localized and Propagating Surface Plasmons in Gold Particles of Near-Micron Size. J. Phys. Chem. C, **2009**, *113*, 40-44.

[23]. Cole, R.M; *, Baumberg, J. J; Garcia de Abajo, F. J.; Mahajan, S; Abdelsalam, M; Bartlett, P.N. Understanding Plasmons in Nanoscale Voids. Nano Letters, **2007**, *7*, 2094-2100.

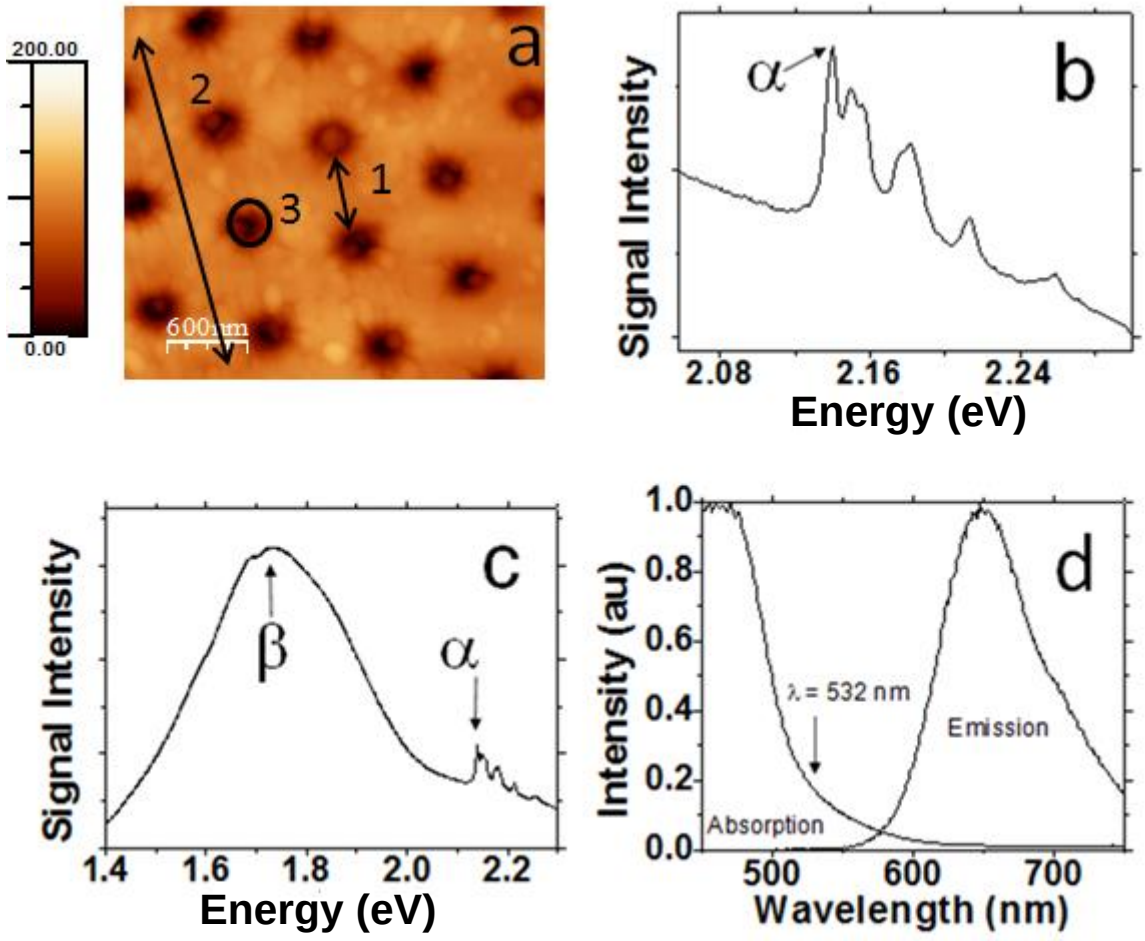

Fig 1. (a) AFM image of the array showing the presence of a regular array of cavities across the sample. The black lines schematically represent examples of 1) shortest distance between nanocavities, 2) a continuous strip of Au between rows of nanocavities, 3) cavity, (b) SERRS spectrum recorded for approx. 10 sec, (c) emission and SERRS spectrum recorded for 10 sec within the same experimental window, λ_{ex}=532 nm, (d) absorption and emission spectra of the dye absorbed into the cavity surface.

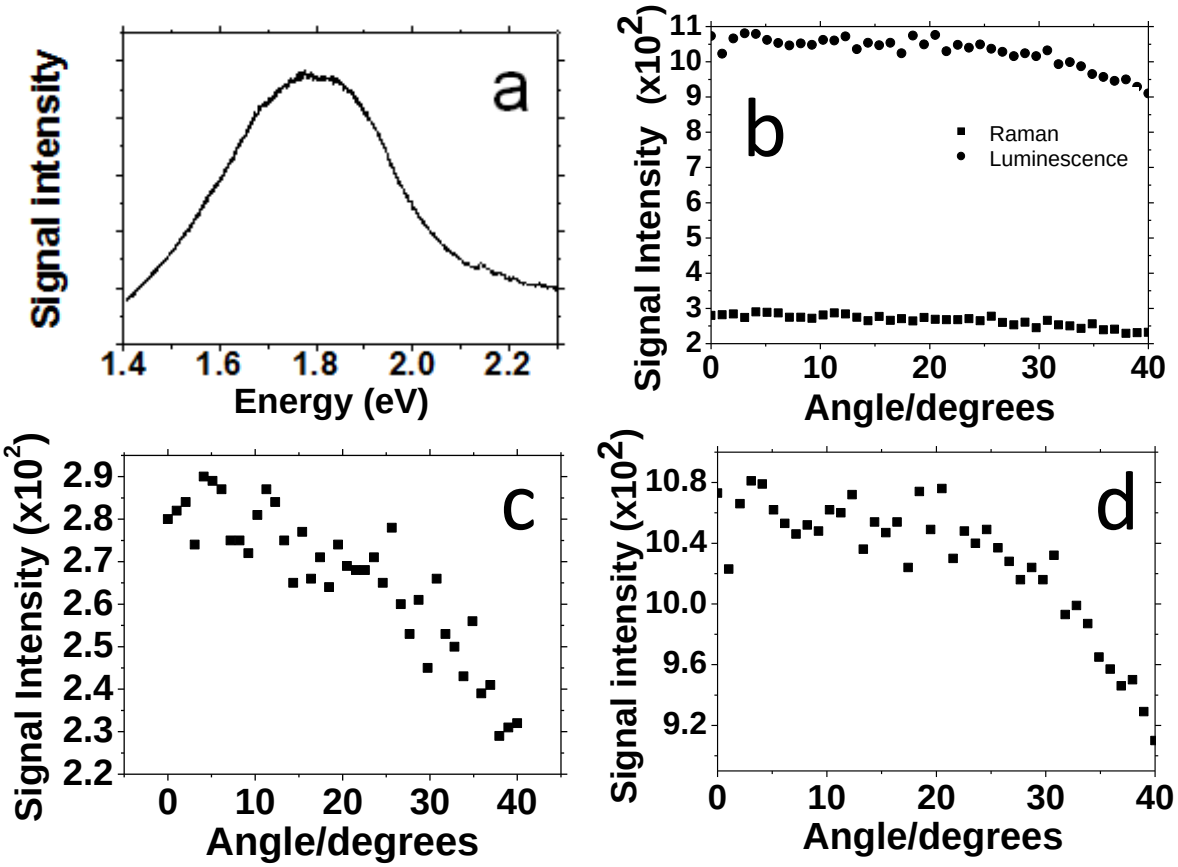

Fig 2. Studies of SERRS and emission from dye placed only within the cavity for the 820 nm nanocavity array, (a) emission and SERRS spectrum recorded for approx. 0.1 sec within the same experimental window, (b) a plot of Raman and emission intensity as a function of angle for the Raman band at 1.7586eV and emission at 1.82 eV, (c) and (d) are plots of the Raman and emission intensity shown in (b) shown again with smaller scales shown for clarity.

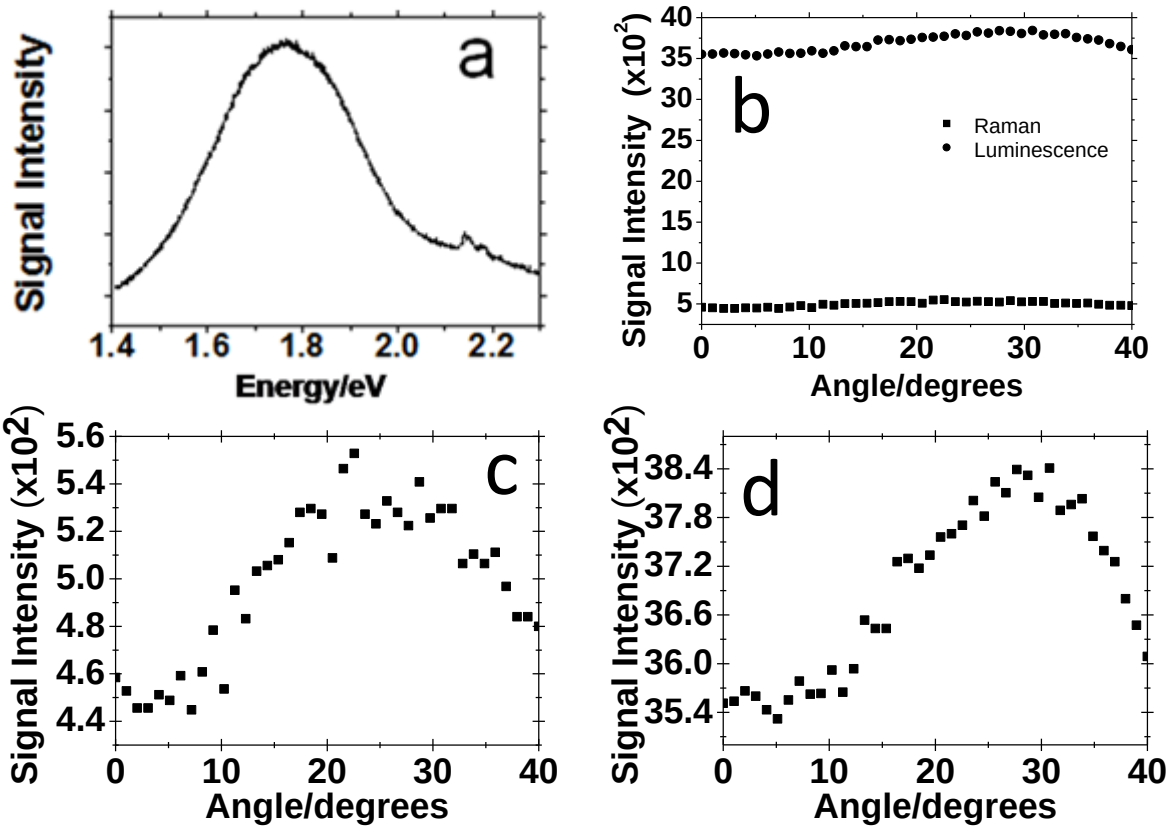

Fig 3. Studies of SERRS and emission from dye placed only on the surface of the 820 nm nanocavity array, (a) emission and SERRS spectrum recorded for approx. 0.1 sec within the same experimental window, (b) a plot of Raman and emission intensity as a function of angle for the Raman band at 1.759eV and emission at 1.82 eV, (c) and (d) are plots of the Raman and emission intensities shown in (b) shown again with smaller scales for clarity.

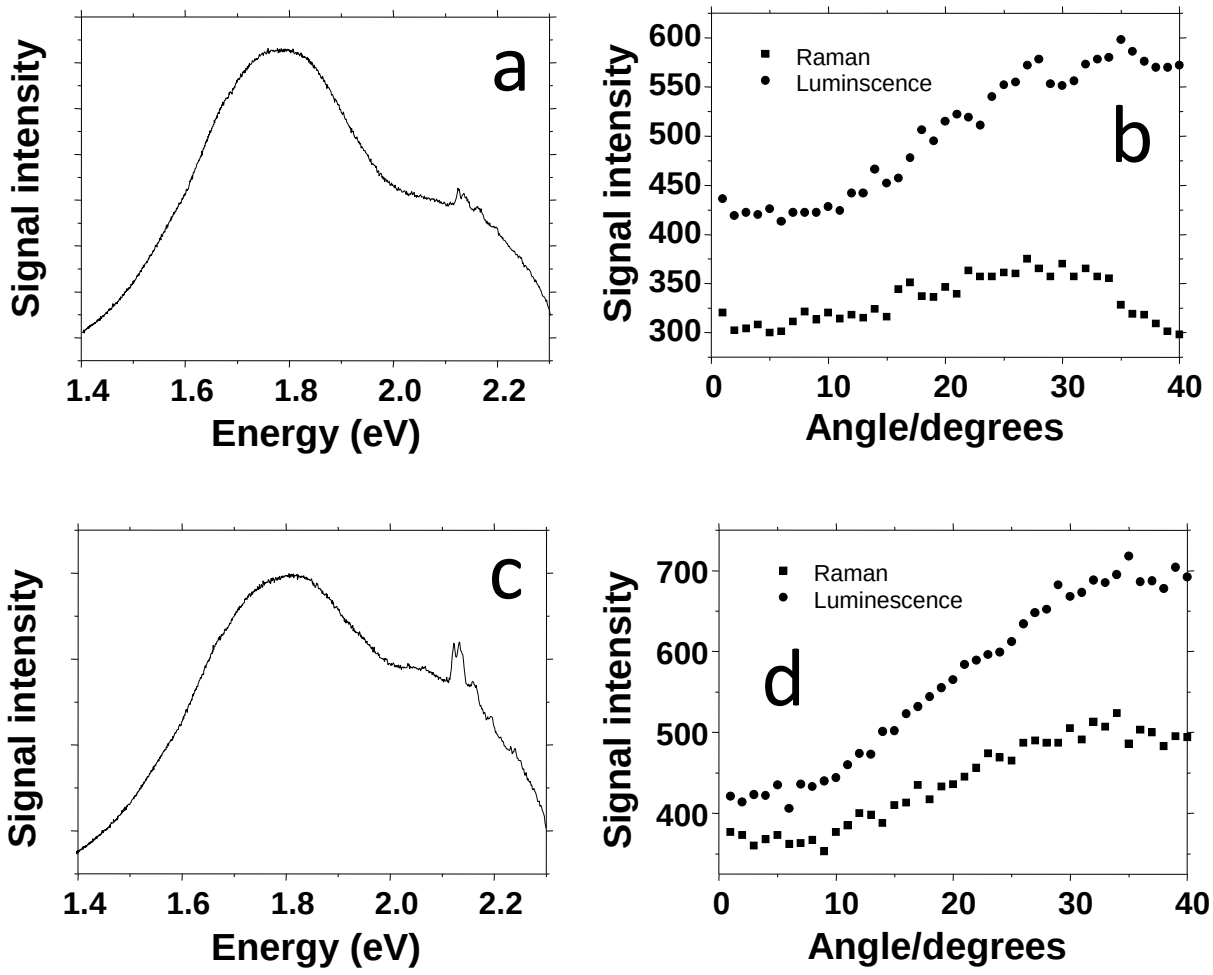

Figure 4. (a-b) Studies of SERRS and emission from molecule placed only within the 430 nm cavity substrate, (a) SEL and SERRS spectrum recorded for approx. 0.1 sec, (b) a plot of SEL and SERRS intensity as a function of angle at 1.82 eV and 1.76eV respectively. (c-d) Studies of SERRS and emission from molecule placed on the surface of the 430 nm cavity substrate, (c) SEL and SERRS spectrum recorded for approx. 0.1 sec, (d) a plot of SEL and SERRS intensity as a function of angle at 1.82 eV and 1.76eV respectively.